Article

Theoretical Study on Geometries of Electrodes in Laboratory Electrical Resistivity Measurement

Chang-Ho Hong [1], Song-Hun Chong [2] and Gye-Chun Cho [1],*

[1] Department of Civil and Environmental Engineering, Korea Advanced Institute of Science and Technology (KAIST), Daehakro 291, Daejeon 34141, Korea; hello-hch@kaist.ac.kr

[2] Department of Civil Engineering, Sunchon National University, Jungang-ro 255, Sunchon, Jeollanam-do 57922, Korea; shchong@scnu.ac.kr

* Correspondence: gyechun@kaist.ac.kr; Tel.: +82-42-350-3622

check for updates

Featured Application: Determination of the container size for electrical resistivity measurement.

Abstract: Electrical resistivity tests have been widely conducted in multiple scales, from a few centimeters to kilometers. While electrode spacing is used to define field resistance, laboratory measurements in a limited space need to consider electrode geometry. However, there are no studies that theoretically explore the effects of the geometries of electrodes and container size on laboratory electrical resistivity measurements. This study formulates a theoretical electrical resistance for the geometry of cylindrical electrodes and the size of a non-conductive container with the method of image charges. As a complementary study, experimental tests were conducted to verify the derived equations. The discussion includes the concepts of the spherical equivalent electrodes and a simple design method for container size.

1. Introduction

The electrical resistivity method is one of the most promising geophysical methods for characterizing subsurface conditions, including soil profiling, anomaly detection, and groundwater chemistry [1–4]. Cylindrical electrodes are usually employed to increase the contact area with the medium, and thus minimize grounding resistance [5,6]. Note that the high ground resistance, induced by imperfect contact, hinders the flow of current into the medium and produces unstable electrical resistance of the medium [7]. In addition, electrical resistivity tests have been widely conducted at diverse scales, from a few centimeters for laboratory-scale tests to kilometers for field tests [8–12]. Large distances among electrodes in field tests force well-known theoretical equations (e.g., Wenner or Schlumberger method) to ignore the geometries of an electrode (radius and penetrated depth) and to only reflect electrode spacing [1,2]. With relatively short electrode spacing (e.g., laboratory tests), the penetrated depth of the electrodes has a significant effect on the electrical resistivity measurements [13,14]. In addition, the distortion of current flow occurs near the container and produces inaccurate electrical resistance [15]. However, previous studies failed to adequately take into account all of the geometries (radius and penetrated depth) of the electrodes, electrode spacing, and container size.

In this study, theoretical electrical resistances are formulated for cylindrical electrode geometries (radius and penetrated depth) and spacing in a container. The method of image charges is adopted

to replace the container geometry with imaginary electrodes and facilitate analyzing the electrical resistivity variation near the container. Then, experimental tests are performed to validate the theoretical equations. The concept of the spherical equivalent electrode is revisited with the proposed formulations. Emphasis is placed on considering the electrode geometries in laboratory-scale measurements.

2. Theoretical Background

2.1. Electric Potential from a Point Electrode

Electrical resistivity is defined by Ohm's law and Gauss's flux theorem. Ohm's law as an empirical equation gives $R = V/I$, where V and I are the potential differences across a resistor and the current passing through it, respectively. Meanwhile, Gauss's flux theorem defines the flow and distribution of an electric charge induced by an electrical field. To formulate the electrical potential of a single electrode, Ohm's law can be alternatively rewritten in terms of the electrical field strength E (volts/m) and current density J (amps/m^2) when the electric field is conservative (i.e., curl $\nabla \times E = 0$)

$$J = \sigma E = \sigma(-\nabla V) \tag{1}$$

where σ is the electrical conductivity of the material (1/Ω·m), V is the electric potential (volts), and ∇ is the del operator. By taking the del operator on both sides of Equation (1), it can be expressed as

$$\nabla \cdot J = -\left(\underbrace{\nabla \sigma \cdot \nabla V}_{=0} + \sigma \nabla^2 V \right) = -\sigma \nabla^2 V = 0 \tag{2}$$

The electrical conductivity in the homogeneous medium keeps constant, and thus the divergence of electrical conductivity becomes zero. The Laplace equation that describes the electrical potential distribution under steady-state conditions can be rewritten with the spherical coordinate system,

$$\nabla^2 V = \frac{1}{s^2} \frac{\partial}{\partial s} \left(s^2 \frac{\partial V}{\partial s} \right) = \frac{\partial^2 V}{\partial s^2} + \left(\frac{2}{s} \right) \frac{\partial V}{\partial s} = 0 \tag{3}$$

where s is the distance from electrode center. By solving the second order Euler differential equation, it can be expressed as

$$V = \frac{C_1}{s} + C_2 \tag{4}$$

Two constants, C_1 and C_2, can be obtained by imposing the boundary condition ($V = 0$ as $s \to \infty$) and using the relation between the current and current density,

$$I = A \cdot J = A \cdot \left(\sigma \cdot -\frac{dV}{ds} \right) = A\sigma \frac{C_1}{s^2} \quad \therefore C_1 = \frac{\rho I}{A} s^2 \tag{5}$$

where A is the equipotential surface area and ρ, as electrical resistivity, has an inverse relation with its conductivity ($=1/\sigma$). Thus, the electric potential gradient (dV/ds) induced by a shaped electrode in the homogeneous half space helps to formulate general electrical potential [16],

$$V = \int \frac{\rho I}{A} ds \tag{6}$$

where A is the equipotential surface area as a function of s, which is the distance from the electrode center line.

2.2. Electrical Resistance Measured between Two Cylindrical Electrodes

We assume that two cylindrical electrodes, with radii *r* and penetration depth *l*, are separated by distance *L*, as seen in Figure 1. These two electrodes have the same amount of charge but opposite polarities. The electric potential of one electrode is calculated from the equipotential surface area in terms of the shortest distance between the electrode center line and an arbitrary point (*s*). The equipotential surface area of one cylindrical electrode is:

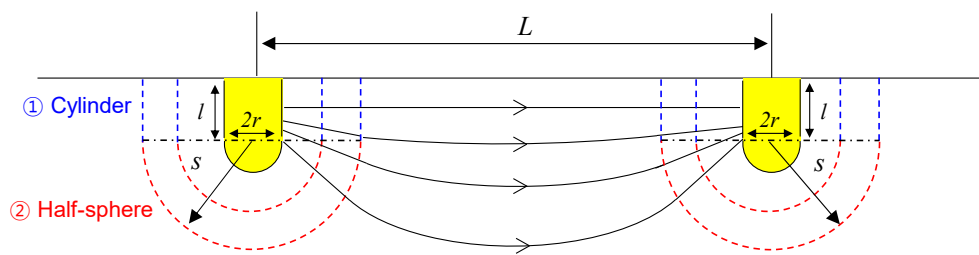$$A(s) = \underbrace{2\pi s l}_{\text{Cylinder side}} + \underbrace{2\pi s^2}_{\text{Half sphere}} \tag{7}$$

Figure 1. Definitions of the symbols and equipotential surface shape between two cylindrical electrodes.

The electric potentials of two cylindrical electrodes are derived from the following equation:

$$V_1 = -V_2 = \int_r^{L-r} \frac{\rho I}{A(s)} ds = \int_r^{L-r} \frac{\rho I}{2\pi s l + 2\pi s^2} ds = \frac{\rho I}{2\pi l}\left[\ln\left(1 + \frac{l}{r}\right) - \ln\left(1 + \frac{l}{L-r}\right)\right] \tag{8}$$

V_1 is the potential of positive polarity, V_2 is the potential of negative polarity, ρ is the electrical resistivity of the material, *I* is the electric current between two electrodes, and *L* is the distance between two cylindrical electrodes.

Through Ohm's law, the electrical resistance between two cylindrical electrodes ($R_{cylindrical}$) is:

$$R_{cylindrical} = \frac{\rho}{\pi l}\left[\ln\left(1 + \frac{l}{r}\right) - \ln\left(1 + \frac{l}{L-r}\right)\right] \tag{9}$$

where ρ is the electrical resistivity of the material, *l* is the penetration depth of the electrodes, *r* is the radius of the electrodes, and *L* is the distance between two electrodes. As the penetration depth approach zero ($l\to0$), Equation (9) can have a mathematical formulation as

$$\lim_{l\to0} R_{cylindrical} = \lim_{l\to0} \frac{\rho}{\pi l}\left[\ln\left(1 + \frac{l}{r}\right) - \ln\left(1 + \frac{l}{L-r}\right)\right]$$

$$= \frac{\rho}{\pi}\left[\frac{1}{r}\ln\left(\underbrace{\lim_{l/r\to0}\left(1 + \frac{l}{r}\right)^{\frac{r}{l}}}_{=e}\right) - \frac{1}{L-r}\ln\left(\underbrace{\lim_{\frac{l}{L-r}\to0}\left(1 + \frac{l}{L-r}\right)^{\frac{L-r}{l}}}_{=e}\right)\right] = \frac{\rho}{\pi}\left[\frac{1}{r} - \frac{1}{L-r}\right] \tag{10}$$

2.3. Two Cylindrical Electrodes in the Container

The method of image charges has been employed to describe electrical and magnetic fields with even and specified boundary conditions. The underlying theorem that explains the uniqueness of the solution facilitates solving a cumbersome Laplace equation. Figure 2 shows the equivalent system by replacing the non-conductive wall of the container embedded with two cylindrical electrodes into image charges of both side-walls. Note that potentials at the side-walls become zero. In the original

system, the current, I, flows from electrode M to electrode N, and the potential difference between electrode M and electrode N in the container can be calculated from Equation (8) and potentials from the imaginary electrodes involved in the electrode geometry and spacing.

$$V_3 = \frac{\rho I}{2\pi l} \left\{ \begin{array}{c} \underbrace{\ln\left(1+\frac{l}{r}\right)}_{\text{effect of M}} + \underbrace{\left(-\ln\left(1+\frac{l}{L-r}\right)\right)}_{\text{effect of N}} \\ + \left[\underbrace{\overset{\text{effect of M}'}{\ln\left(1+\frac{l}{W-L-r}\right)} + \overset{\text{effect of N}'}{\left(-\ln\left(1+\frac{l}{W-r}\right)\right)} + \overset{\text{effect of M}''}{\ln\left(1+\frac{l}{W+L-r}\right)} + \overset{\text{effect of N}''}{\left(-\ln\left(1+\frac{l}{W-r}\right)\right)}}_{\text{effect of container wall}} \right] \end{array} \right\}$$

(11)

$$V_4 = \frac{\rho I}{2\pi l} \left\{ \begin{array}{c} \underbrace{-\ln\left(1+\frac{l}{r}\right)}_{\text{effect of N}} + \underbrace{\ln\left(1+\frac{l}{L-r}\right)}_{\text{effect of M}} \\ + \left[\underbrace{\overset{\text{effect of N}'}{-\ln\left(1+\frac{l}{W+L-r}\right)} + \overset{\text{effect of M}'}{\ln\left(1+\frac{l}{W-r}\right)} + \overset{\text{effect of N}''}{\left(-\ln\left(1+\frac{l}{W-L-r}\right)\right)} + \overset{\text{effect of M}''}{\ln\left(1+\frac{l}{W-r}\right)}}_{\text{effect of container wall}} \right] \end{array} \right\}$$
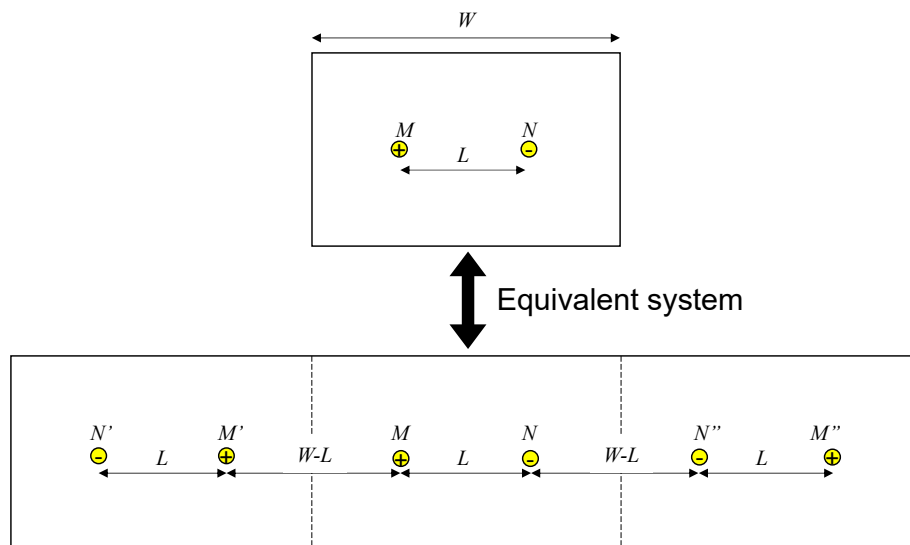
(12)

Figure 2. Basic concept of imaginary electrodes.

The theoretical resistance of the cylindrical electrodes in a non-conductive container is:

$$R_{boundary} = \frac{V_3 - V_4}{I} = \frac{\rho}{\pi l} \left\{ \begin{array}{c} \underbrace{\ln\left(1+\frac{l}{r}\right)}_{\text{effect of an electrode}} + \underbrace{\left(-\ln\left(1+\frac{l}{L-r}\right)\right)}_{\text{effect of the other electrode}} \\ + \left[\underbrace{\ln\left(1+\frac{l}{W+L-r}\right) + \ln\left(1+\frac{l}{W-L-r}\right) - 2\ln\left(1+\frac{l}{W-r}\right)}_{\text{effect of container wall}} \right] \end{array} \right\}$$

(13)

where *W* is the width of the container.

Only two boundaries vertical, to the electrodes' movement direction, are considered in Equation (13) because the distance to the other boundaries is constant and far enough from the electrodes. In addition, the electrical resistivity of the boundaries is assumed as an infinite since the electrical resistivity of the acrylic is much higher than that of the brine.

3. Experimental Tests and Results

Experimental tests were conducted for verification of the derived equations in the previous section. A brine was selected as the material, and its electrical resistivity was measured during the experimental tests. Two brines were prepared by adding 2.16 g and 8.64 g of sodium chloride (NaCl) to distilled water (0.005 and 0.02 mol/L) and stirred over 5 min at 20 °C. The corresponding electrical resistivities of the brines were 18.88 and 4.78 $\Omega\cdot m$, respectively. The test setup is depicted in Figure 3. The container was made of acrylic and its size was $0.275 \times 0.215 \times 0.13$ m; the brine is filled up to 0.125 m in height (the volume of the brine = 7.39 L). Cylindrical electrodes, with a radius (*r*) of 4 mm and height of 50 mm, were made of SUS303 to prevent corrosion and rubber rings were utilized to control and maintain the penetration depth of the electrodes. The electrical resistivity of the brine and the electrical resistance between the two electrodes were measured with a conductivity meter (Mettler Toledo S213, Mettler Toledo, Columbus, OH, USA) and LCR meter (Agilent HP 4263B, Agilent, Santa Clara, CA, USA) which can measure inductance, capacitance and resistance. A 1-V signal was applied, which was the maximum voltage of the measurement equipment, and a 1-kHz signal, which is the most commonly utilized frequency in petrophysics and other engineering fields, was applied to avoid the polarization effect [17,18]. The electrical resistance was measured by varying the penetration depth (*l*) and the distance between the two electrodes (*L*). Experimental test cases are listed in Table 1.
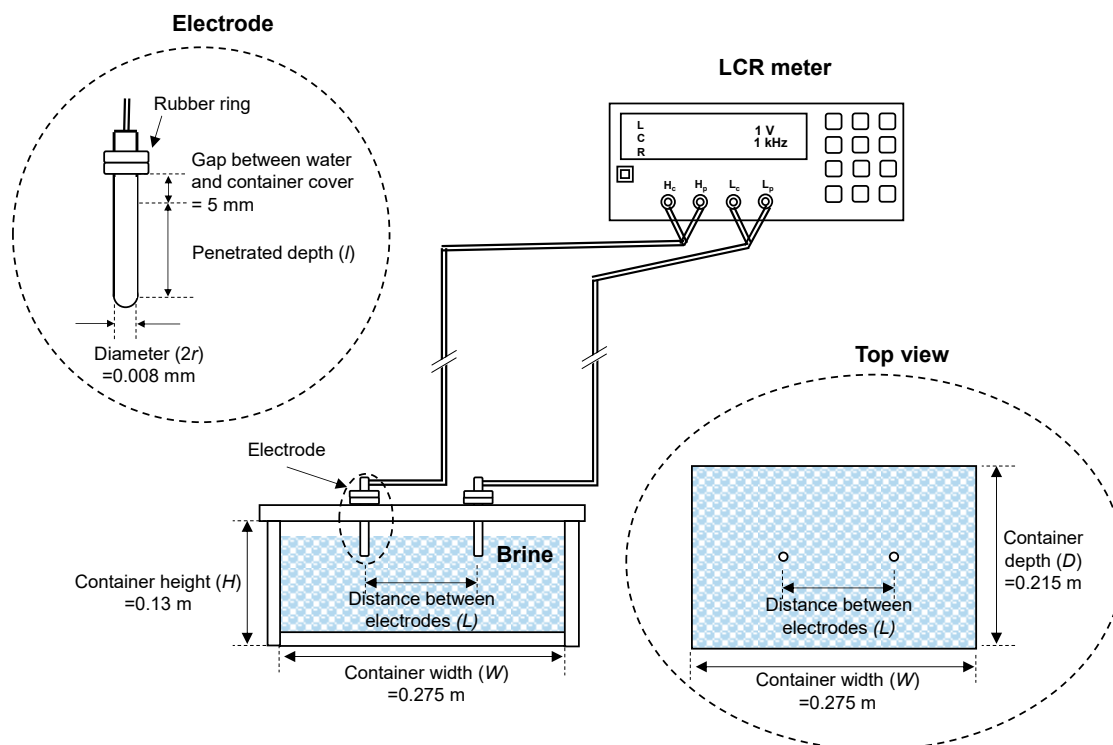

Figure 3. Test setup: measurement equipment, container and electrodes.

Table 1. List of experimental test cases.

Electrical Resistivity, ρ (Ωm)	Penetration Depth, l (mm)	Distance between Two Electrodes, L (m)
18.88	0	0.015
		0.045
	4	0.085
4.78	8	0.125
		0.165
	16	0.205
		0.245

Figure 4 shows the theoretical and experimental resistances, as a function of the distance between electrodes (L), in a brine with an electrical resistivity of 18.88 Ωm. Lower electrical resistivity produced a higher current flowing through the brine (lower electrical resistance). Additionally, a deeper penetration depth (larger contact area of the electrode) resulted in a lower measured resistance. The predicted resistance from Equations (9) and (10) have a strong correlation until $L = 0.165$ m with the measured electrical resistance. However, the measured electrical resistance suddenly increased relative to the predicted value from $L = 0.205$ m. The deviation was attributed to the electrical boundary effect that results from distortion of the electric current near the boundaries. A similar phenomenon was reported in the previous research utilizing the non-conductive polycarbonate container for the experimental tests [18]. The authors stated that the container boundary affects the current flow during the electrical resistivity measurement. Note that the container in this study was made from a non-conductive material (acryl). The dashed line obtained from Equation (13), reflecting the container wall effect, gives an accurate prediction near the container wall. This means that the electrical resistivity of the acrylic is much higher than that of the brine, as assumed in the formulation process.
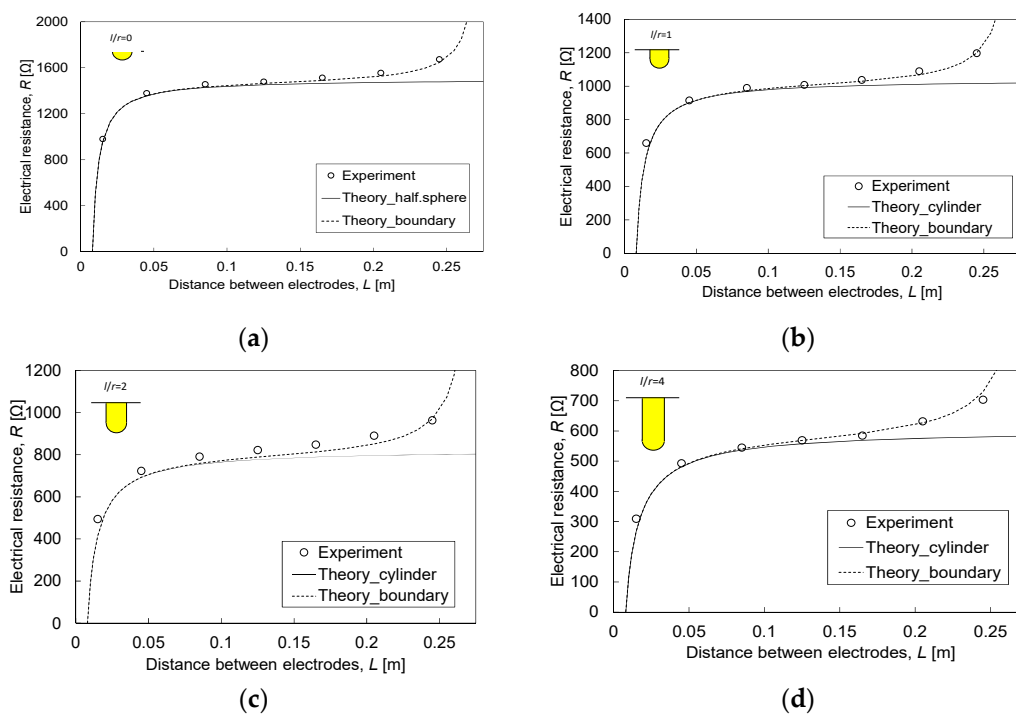

Figure 4. Evolution of electrical resistance with distance and depth (18.88 Ωm): (**a**) $l/r = 0$, (**b**) $l/r = 1$, (**c**) $l/r = 2$, and (**d**) $l/r = 4$. Continuous lines are obtained from Equation (9) and dashed lines are obtained from Equation (13).

4. Discussion

4.1. Electrical Resistance Measured between Two Half-Buried Spherical Electrodes

Herein, we assume two half-buried spherical electrodes, equal in radius (r) and quantity of charge but opposite in polarity, are separated by the distance L (Figure 5). The electric potential of an arbitrary point, situated at a distance s from the electrodes, is obtained from the equipotential surface area ($A(s)$):

$$V_5 = -V_6 = \int_r^{L-r} \frac{\rho I}{A(s)} ds = \int_r^{L-r} \frac{\rho I\, ds}{\underbrace{2\pi s^2}_{\substack{\text{surface area of}\\\text{half-sphere}}}} = \frac{\rho I}{2\pi}\left(\frac{1}{r} - \frac{1}{L-r}\right) \tag{14}$$

where V_5 is the electric potential from the positive-charge electrode and V_6 is the electric potential from the negative-charge electrode. I is the electric current between the two electrodes, and ρ is the electrical resistivity of the material. The equipotential surface area of the half-spherical electrodes is identical to that of the point electrodes in the previous section.
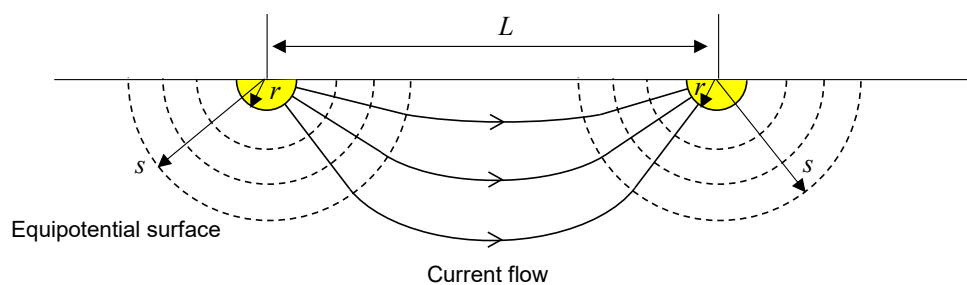

Figure 5. Definitions of the symbols and equipotential surface shape between two half-buried spherical electrodes.

Through Ohm's law, the electrical resistance between two half-spherical electrodes ($R_{half\text{-}sphere}$) is:

$$R_{half-sphere} = \frac{V_5 - V_6}{I} = \frac{\rho}{\pi}\left(\frac{1}{r} - \frac{1}{L-r}\right) \tag{15}$$

This is identical to Equation (10) and the 3D resistance reported in Reference [19]. If the distance between the two electrodes increases, the electrical resistance between them continuously increases (the derivative of $R_{half\text{-}sphere}$ about L is always positive) and finally becomes $\rho/\pi r$, as reported by many researchers [20,21]. Additionally, the electrical resistance becomes zero when the two electrodes are in contact with each other ($L = 2r$).

Even though the cylindrical electrodes are commonly utilized, not all of the electrodes for the electrical resistivity measurement are cylindrically shaped [22–25]. The concept of equivalent electrodes is revisited and commonly adopted for a simple calculation of the shaped electrodes. The shapes of the equivalent electrodes become half-spheres which have the same surface area as the original electrodes. The radius of the equivalent electrodes (r_e), for the cylindrical electrodes with spherical tips, can be seen as

$$2\pi r_e^2 = 2\pi r l + 2\pi r^2 \Rightarrow r_e = r\sqrt{1 + \frac{l}{r}} \tag{16}$$

$$R_{equivalent}/R_{cylinderical} = \frac{l}{r}\left(\frac{1}{\sqrt{1+\frac{l}{r}}} - \frac{1}{\frac{L}{r} - \sqrt{1+\frac{l}{r}}}\right)\bigg/\left[\ln\left(1+\frac{l}{r}\right) - \ln\left(1+\frac{\frac{l}{r}}{\frac{L}{r}-1}\right)\right] \tag{17}$$

Figure 6 displays the electrical resistance between two cylindrical electrodes (Equation (8), solid line) and between two equivalent electrodes (Equation (15) using Equation (16), dashed line) in a brine with an electrical resistivity of 4.78 Ωm. It is trivial that the radius of the equivalent electrode is bigger than that of the cylindrical electrode from Equation (16). Therefore, the distance between electrodes that makes the electrical resistance zero in Figure 6 is slightly larger in the case of the equivalent electrodes. The gap between the solid and dashed line decreases as the ratio between the penetration depth and the radius (l/r) decreases and increases when l/r increases and converges. Figure 7 depicts the relationship between L/r, l/r, and $R_{equivalent}/R_{cylinderical}$ using Equation (17). If one were to treat the cylindrical electrodes as half-buried spherical electrodes, Figure 6 could be used as a guideline for determining the allowable error. For instance, if the allowed error is 2% (0.98–1.02 in *y*-axis of Figure 7) and l/r is determined as 2, L/r should exist from 8 to 11.
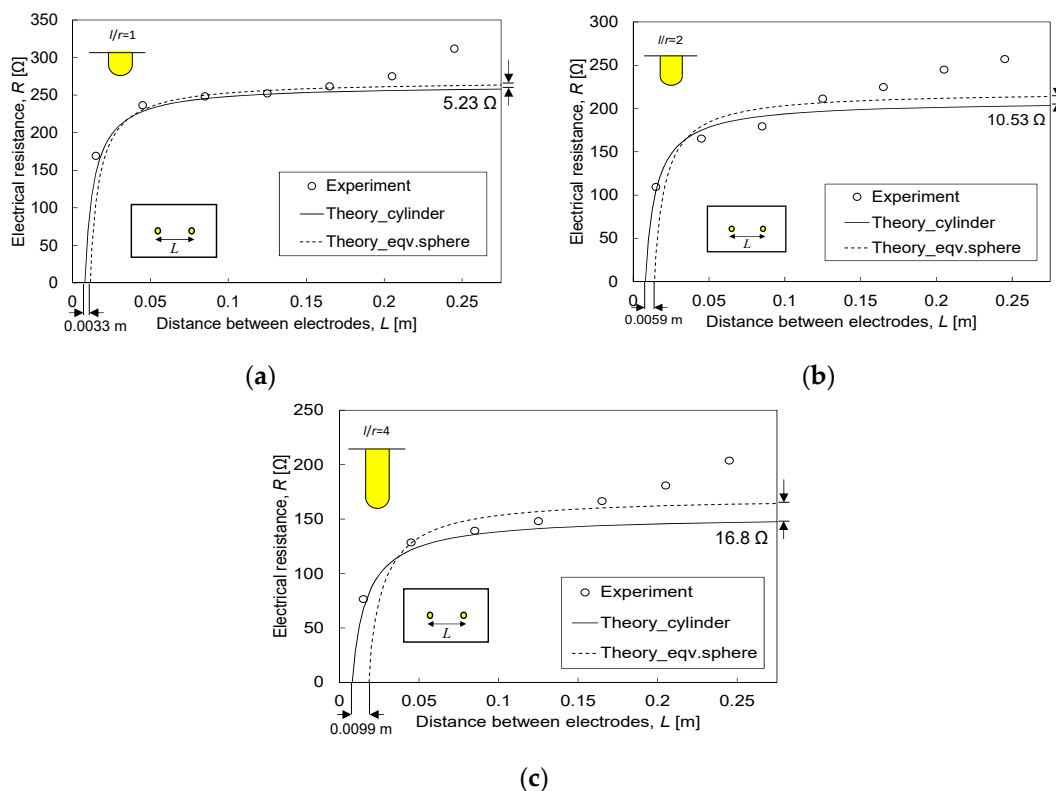

(a)

(b)

(c)

Figure 6. Experimental test results (4.78 Ωm): (**a**) $l/r = 1$, (**b**) $l/r = 2$, and (**c**) $l/r = 4$. Continuous lines are obtained from Equation (9) and dashed lines are gained from Equation (15) by replacing *r* from Equation (16).

4.2. Parametric Study: Influence of the Electrode Geometry on Boundary Effect

A parametric study was conducted to explore the effect of cylindrical electrode geometries and container size. The initial conditions of the electrodes and the medium were assumed as $r = 0.001$ m, $l = 0.01$ m, $L = 0.1$ m and $W = 0.3$ m. The electrical resistance (R) obtained by the given container size was normalized using the electrical resistance at the infinite boundary condition (R_∞). The input parameters are tabulated in Table 2. Figure 8 shows the variation of the normalized electrical resistance. As the W/L increases, the normalized resistance decreases and the boundary effect becomes negligible in all cases. The slender (large l/r) and more spaced (large L/l) electrodes rapidly diminish the boundary effect. The theoretical equation can be used to design the container size for electrical resistivity measurements. For example, once the electrode geometries (l/r) are given, the minimum container size and maximum electrode distance can be simply determined.
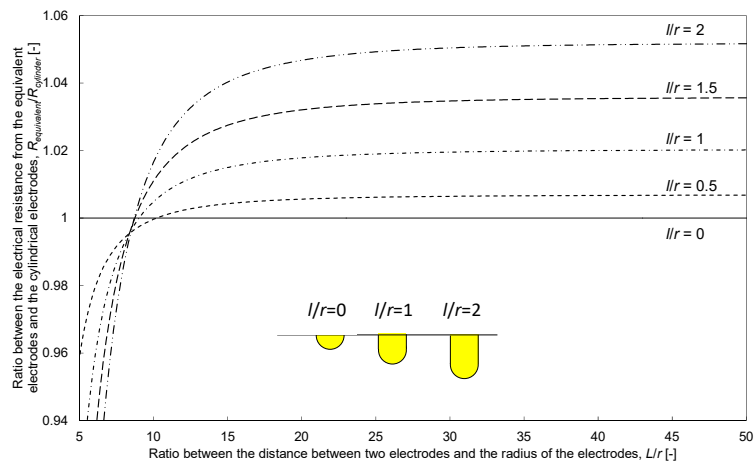
Figure 7. Effect of *l/r* and *L/r* on the electrical resistance between two equivalent electrodes.
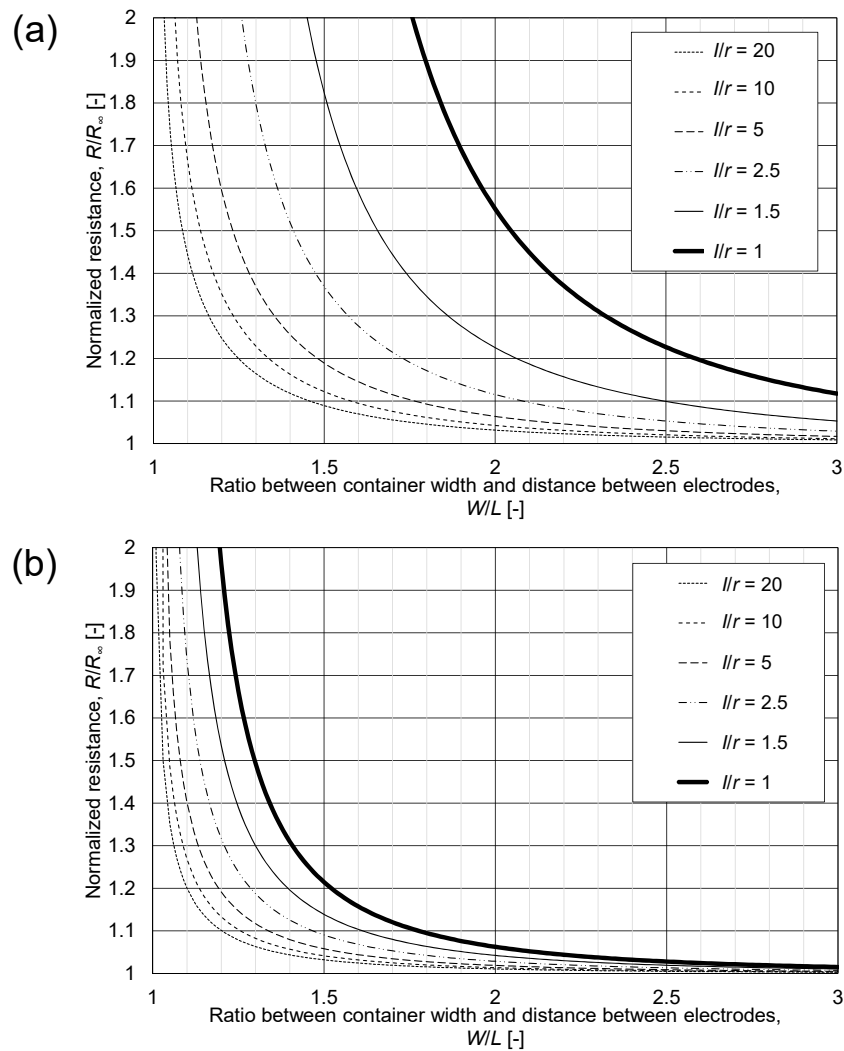

Figure 8. Variation of normalized resistance with respect to electrode geometries and container size: (**a**) *L/l* = 3 and (**b**) *L/l* = 10. Lines are obtained from Equation (13).

Table 2. Parametric study (*r* is the radius of the cylindrical electrodes, *l* is the penetrated depth of the cylindrical electrodes, *L* is the distance between two cylindrical electrodes).

l/r (-)	*L/l* (-)
1	
1.5	
2.5	3
5	10
10	
20	

5. Conclusions

In this study, the theoretical electrical resistance of cylindrical electrodes was derived for finite and infinite mediums, using equipotential surface area for the characterization of the materials. Because the radius, penetration depth, and position of the electrodes affect electrical resistance, experimental tests were performed for the verification of the theoretical equations. The conclusions obtained from this study are as follows:

1. The theoretical electrical resistance, between two cylindrical electrodes with rounded tips, is represented as a function of the radius (*r*) and penetration depth (*l*) of the electrodes and the distance (*L*) between the two electrodes. The electrical resistance increases when the electrical resistivity of the material and the distance between the electrodes increase and the radius and penetration depth decrease.
2. Over short distances, the measured electrical resistance between two cylindrical electrodes shows a similar tendency to values predicted by the theoretical equation. However, as the distances increase, the electrodes are situated closer to the non-conductive (acrylic) walls of the container and the measured electrical resistance is higher than the predicted values. This boundary effect is caused by the distortion of the current flow near the non-conductive materials and it starts in about a quarter of the container width from the container wall. The boundary effect is adjusted by adopting the method of image charges.
3. It is verified that the electrical resistance between two cylindrical electrodes becomes identical to the electrical resistance between two half-buried spherical electrodes as the penetration depth becomes shallow. The cylindrical electrodes can be treated as half-buried spherical electrodes with the allowable error range. If the allowable error of the measured electrical resistance is 2%, the ratio between penetration depth and the radius is less than unity.
4. The parametric study shows that the boundary effect can be reduced when the ratio between the penetration depth and the radius (*l/r*) and the spacing and the penetration depth (*L/l*) are large. Therefore, it is recommended to employ slender electrodes or a short distance between two electrodes to avoid the boundary effect in a fixed size container.

References

1. Wenner, F. The four-terminal conductor and the Thomson bridge. *Bull. Bur. Stand.* **1912**, *8*, 559–610. [CrossRef]
2. Tagg, G.F. *Earth Resistances*; Pitman Pub. Corp.: New York, NY, USA, 1964.

3. Telford, W.M.; Geldart, L.P.; Sheriff, R.E. *Applied Geophysics*, 2nd ed.; Cambridge University Press: Cambridge, UK, 1990.

4. Byun, Y.K.; Hong, W.T.; Yoon, H.K. Characterization of cementation factor of unconsolidated granular materials through time domain reflectometry with variable saturated conditions. *Materials* **2019**, *12*, 1340. [CrossRef] [PubMed]

5. Rücker, C.; Günther, T. The simulation of finite ERT electrodes using the complete electrode model. *Geophysics* **2011**, *76*, 227–238. [CrossRef]

6. Rooney, W.J.; Gish, O.H. Results of Earth-resistivity surveys near Watheroo, Western Australia, and at Ebro, Spain. *Terr. Magn. Atmos. Electr.* **1927**, *32*, 49–63. [CrossRef]

7. Ingeman-Nielsen, T.; Tomaškovičová, S.; Dahlin, T. Effect of electrode shape on grounding resistances—Part 1: The focus-one protocol. *Geophysics* **2016**, *81*, WA159–WA167. [CrossRef]

8. Daily, W.; Ramirez, A.; Binley, A. Remote monitoring of leaks in storage tanks using electrical resistance tomography: Application at Hanford site. *J. Environ. Eng. Geophys.* **2004**, *9*, 11–24. [CrossRef]

9. Rücker, C.; Günther, T.; Spitzer, K. Three-dimensional modelling and inversion of dc resistivity data incorporating topography—I. Modelling. *Geophys. J. Int.* **2006**, *166*, 495–505. [CrossRef]

10. Binley, A.; Henry-Poulter, S.; Shaw, B. Examination of solute transport in an undisturbed soil column using electrical resistance tomography. *Water Resour. Res.* **1996**, *32*, 763–769. [CrossRef]

11. Igel, J. *On the Small-Scale Variability of Electrical Soil Properties and its Influence on Geophysical Measurements*; University of Frankfurt/Main: Frankfurt, Germany, 2007.

12. Flechsig, C.; Fabig, T.; Rücker, C.; Schütze, C. Geoelectrical investigations in the Cheb Basin/W-Bohemia: An approach to evaluate the near-surface conductivity structure. *Stud. Geophys. Geod.* **2010**, *54*, 443–463. [CrossRef]

13. Baishiki, R.S.; Osterberg, C.K.; Dawalibi, F. Earth Resistivity Measurements Using Cylindrical Electrodes at Short Spacings. *IEEE Trans. Power Deliv.* **1987**, *2*, 64–71. [CrossRef]

14. Taiwo, S.M.; Lee, J.S.; Yoon, H.K. Analytical and experimental studies to obtain electrical resistivity in a small-scaled laboratory test. *Geophysics* **2017**, *82*, 267–275. [CrossRef]

15. Park, J.; Lee, K.H.; Seo, H.; Ryu, J.; Lee, I.M. Role of induced electrical polarization to identify soft ground/fractured rock conditions. *J. Appl. Geophys.* **2017**, *137*, 63–72. [CrossRef]

16. Van Nostrand, R.G.; Cook, K.L. *Interpretation of Resistivity Data*; United States Government Printing Office: Washington, DC, USA, 1966.

17. Glover, P.W.; Hole, M.J.; Pous, J. A modified Archie's law for two conducting phases. *Earth Planet. Sci. Lett.* **2000**, *180*, 369–383. [CrossRef]

18. McCarter, W.J.; Starrs, G.; Kandasami, S.; Jones, R.; Chrisp, T. Electrode configurations for resistivity measurements on concrete. *Aci. Mater. J.* **2009**, *106*, 258–264.

19. Jaschinsky, P.; Wensorra, J.; Lepsa, M.I.; Mysliveček, J.; Voigtländer, B. Nanoscale charge transport measurements using a double-tip scanning tunneling microscope. *J. Appl. Phys.* **2008**, *104*, 094307. [CrossRef]

20. Blythe, A. Electrical resistivity measurements of polymer materials. *Polym. Test.* **1984**, *4*, 195–209. [CrossRef]

21. Ryu, H.H. *Development of Tunnel Electrical Resistivity Prospecting System and its Application*; Korea Advanced Institute of Science and Technology (KAIST): Daejeon, Korea, 2010.

22. Moussa, A.H.; Dolphin, L.T.; Mokhtar, G. *Applications of Modern Sensing Techniques to Egyptology*; A report of the 1977 Field Experiments by a Joint Team; SRI International: Menlo Park, CA, USA, 1977.

23. Athanasiou, E.; Tsourlos, P.; Vargemezis, G.; Papazachos, C.; Tsokas, G. Non-destructive DC resistivity surveying using flat-base electrodes. *Near Surf. Geophys.* **2007**, *5*, 263–272. [CrossRef]

24. Won, I. The geometrical factor of a marine resistivity probe with four ring electrodes. *IEEE J. Ocean. Eng.* **1987**, *12*, 301–303. [CrossRef]

25. Ridd, P. Electric potential due to a ring electrode. *IEEE J. Ocean. Eng.* **1994**, *19*, 464–467. [CrossRef]